

# Bures-Wasserstein Importance-Weighted Evidence Lower Bound: Exposition and Applications

Peiwen Jiang

*The University of Sydney Business School, Australia*

Takuo Matsubara

*School of Mathematics, The University of Edinburgh, UK*

Minh-Ngoc Tran

*The University of Sydney Business School, Australia*

## Abstract

The Importance-Weighted Evidence Lower Bound (IW-ELBO) has emerged as an effective objective for variational inference (VI), tightening the standard ELBO and mitigating the mode-seeking behaviour. However, optimizing the IW-ELBO in Euclidean space is often inefficient, as its gradient estimators suffer from a vanishing signal-to-noise ratio (SNR). This paper formulates the optimisation of the IW-ELBO in Bures-Wasserstein space, a manifold of Gaussian distributions equipped with the 2-Wasserstein metric. We derive the Wasserstein gradient of the IW-ELBO and project it onto the Bures-Wasserstein space to yield a tractable algorithm for Gaussian VI. A pivotal contribution of our analysis concerns the stability of the gradient estimator. While the SNR of the standard Euclidean gradient estimator is known to vanish as the number of importance samples  $K$  increases, we prove that the SNR of the Wasserstein gradient scales favourably as  $\Omega(\sqrt{K})$ , ensuring optimisation efficiency even for large  $K$ . We further extend this geometric analysis to the Variational Rényi Importance-Weighted Autoencoder bound, establishing analogous stability guarantees. Experiments demonstrate that the proposed framework achieves superior approximation performance compared to other baselines.

**Keywords:** Variational Inference, Wasserstein Space, Optimal Transport, Wasserstein Gradient Descent

## 1 Introduction

A primary challenge in Bayesian inference often lies in the computation, as practitioners must approximate posterior distributions known only up to normalising constants. Driven by increasingly sophisticated statistical models, the posterior distributions encountered in modern applications have become progressively high-dimensional and complex. This computational burden has motivated the development of scalable alternatives to classical sampling methods. Recent advances largely centre on two optimisation-based approaches: variational inference (VI) and Wasserstein gradient flow (WGF). VI (Jordan et al., 1999) seeks the best approximation of a target distribution from a family of tractable densities, typically parameterized by a vector of variational parameters. For example, Gaussian VI, arguably the most common class of VI, employs a family of Gaussian densities and optimises the mean and covariance by maximising the evidence lower bound (ELBO). In contrast, WGF (Jordan et al., 1998) characterises the dynamics of particles, or random variables, such that

their law minimises a divergence from the target density. WGF offers an elegant geometric foundation, under which the approximation of target densities is formally understood as an infinite-dimensional optimisation over the space of probability distributions.

Recent literature has made significant progress in unifying the distinct paradigms of parametric VI and non-parametric WGF. Notably, Lambert et al. (2024) demonstrated that Gaussian VI can be formulated as a WGF restricted to the space of Gaussian distributions. The core principle involves equipping the space of Gaussian distributions with the 2-Wasserstein metric. The resulting metric space, called the Bures-Wasserstein (BW) space, bridges the differential calculus in the parameter space with that in the space of distributions. This unification facilitates novel theoretical insights and implementations for Gaussian VI by incorporating convex optimization techniques from WGF into VI. For instance, Diao et al. (2023) developed an efficient algorithm for Gaussian VI by adapting the forward-backward scheme originally designed for WGF. They demonstrated that this approach achieves the fastest known convergence rate for Gaussian VI.

Parallel to these developments, the importance-weighted evidence lower bound (IW-ELBO) has garnered significant attention in the context of parametric VI. The IW-ELBO, originally proposed for training variational autoencoders (Burda et al., 2016), has emerged as a compelling objective function of VI alternative to standard ELBO. The ‘mode-seeking’ property of the standard ELBO is a well-recognised limitation, often causing the variational approximation to underestimate the tails of the target density. The IW-ELBO mitigates this issue by constructing a tighter lower bound of the evidence (i.e. the marginal log-likelihood), utilising multiple sets of samples drawn from the variational density. The lower bound constructed by the IW-ELBO approaches the true marginal likelihood as the number of sample sets increases. Recent literature has extensively investigated the statistical properties of the IW-ELBO (Rainforth et al., 2018; Tan et al., 2020; Daudel et al., 2023).

Despite the significant success of the IW-ELBO in VI, its connection to the WGF framework has yet to be established. This paper advances the intersection of IW-ELBO and WGF; our main contributions are summarised as follows:

**Wasserstein Gradient** The Wasserstein gradient is a fundamental component of WGF, defining the steepest descent direction of a functional over probability distributions. We derive the Wasserstein gradient of the IW-ELBO, elucidating its distinction from the standard Euclidean gradient. The Wasserstein gradient is often computationally intractable in practice. We further derive the Bures-Wasserstein gradient of the IW-ELBO, a projection of the Wasserstein gradient onto the BW space, yielding a computationally tractable gradient for Gaussian VI under the Wasserstein geometry.

**Signal-to-Noise Ratio** The optimisation of the IW-ELBO is known to be inefficient when the number of importance samples, denoted by  $K$ , is large. Notably, Rainforth et al. (2018) demonstrated that the *signal-to-noise ratio* (SNR) of the standard Euclidean gradient of the IW-ELBO diminishes as  $K$  increases. This degradation in SNR implies high relative variance in the gradient estimation, rendering the optimisation of the IW-ELBO unstable. We prove that the Wasserstein gradient of the IW-ELBO does not suffer from this degeneration. Remarkably, the SNR of the Wasserstein gradient scales favourably at a rate of  $\Omega(\sqrt{K})$ , making the gradient estimation stable as  $K$  increases.

**Bures-Wasserstein IW-ELBO VI** We provide an efficient algorithm of Gaussian VI for the IW-ELBO, drawing inspiration from the standard Euler discretisation of WGF. We demonstrate the

mass-covering capability of our variational approximation, which effectively approximates target densities, mitigating the tail underestimation inherent in standard Gaussian VI. We evaluate the performance of our implementation through a range of empirical experiments.

**Extension to Generalised Bounds** Finally, we extend our analysis and implementation to the Variational Renyi Importance-Weighted Autoencoder (VR-IWAE) bound (Daudel et al., 2023), another nascent generalisation of the ELBO. Similarly to the IW-ELBO, the VR-IWAE bound exhibits desirable properties over the standard ELBO. We derive the Wasserstein gradient of the VR-IWAE bound, and establish that its SNR also scales as  $\Omega(\sqrt{K})$ . Furthermore, we provide a corresponding algorithm of Gaussian VI for the VR-IWAE bound on the BW space.

The remainder of the paper is organised as follows. Section 2 reviews the necessary background on VI and WGF. Section 3 derives the Wasserstein and Bures-Wasserstein gradients of the IW-ELBO, formulating the objective as a functional over probability distributions. This section then investigates the theoretical properties of the Wasserstein gradient of the IW-ELBO. Subsequently, a practical Gaussian VI algorithm with the IW-ELBO is introduced, leveraging the WGF formulation. Section 4 presents empirical experiments validating the performance of our framework. Finally, Section 5 extends our analysis to the VR-IWAE bound, followed by concluding remarks in Section 6.

## 2 Preliminaries

This section concisely summarises preliminaries of VI, IW-ELBO, and WGF, useful for the development of our methodology. It is convenient to first introduce a set of notations.

**Setup and Notation** Denote by  $\|\cdot\|$  and  $\langle \cdot, \cdot \rangle$  the standard norm and inner-product in  $\mathbb{R}^d$ . Denote by  $\mathbf{S}^d$  the space of  $d \times d$  symmetric matrices. Let  $\mathcal{P}_2(\mathbb{R}^d)$  be the space of probability measures on  $\mathbb{R}^d$  with a finite second moment. For a measurable map  $T : \mathbb{R}^d \rightarrow \mathbb{R}^d$ , denote by  $T_\# \mu$  the push-forward measure of  $\mu$  through  $T$ . For sequences of positive numbers  $a_n$  and  $b_n$ , we write  $a_n = O(b_n)$  ( $a_n = \Omega(b_n)$ ) if there exists a constant  $c > 0$  such that  $a_n/b_n \leq c$  ( $a_n/b_n \geq c$ , respectively) for all  $n$  sufficiently large. Similarly, we write  $a_n = o(b_n)$  if  $a_n/b_n \rightarrow 0$  as  $n \rightarrow \infty$ .

### 2.1 Variational Inference

Many statistical models often involve unobserved latent variables  $z \in \mathcal{Z}$ , used to explain the structure within observed data  $x$ . Typically, the latent variable  $z$  is the parameter of a model, such as the mean and variance of a Gaussian model. These models postulate a joint distribution  $p(x, z)$  of  $x$  and  $z$ . VI offers a scalable framework to approximate the posterior  $p(z|x)$  given data  $x$ , using a density  $q_\psi(z)$ , called *variational distribution*, with a learnable variational parameter  $\psi$ . It optimises the variational distribution  $q_\psi(z)$  through maximisation of the ELBO.

Originally, the ELBO is derived as a lower bound of the marginal log likelihood  $\log p(x)$  as follows:

$$\text{ELBO}(q_\psi) := \mathbb{E}_{z \sim q_\psi} \left[ \log \left( \frac{p(x, z)}{q_\psi(z)} \right) \right] \leq \log \int_{\mathcal{Z}} \frac{p(x, z)}{q_\psi(z)} q_\psi(z) dz = \log p(x).$$

This lower bound results in the following key decomposition

$$\log p(x) = \text{ELBO}(q_\psi) + \text{KL}(q_\psi(z) || p(z|x)),$$

where the last term is the Kullback-Leibler (KL) divergence of the variational distribution  $q_\psi(z)$  from the posterior  $p(z|x)$ . Since the marginal log likelihood  $\log p(x)$  is constant with respect to  $\psi$ , this implies that maximizing  $\text{ELBO}(q_\psi)$  is equivalent with minimizing the KL divergence  $\text{KL}(q_\psi(z)||p(z|x))$ . Importantly, the former is computable, despite that the latter is not because of the dependency on the normalisation constant of the posterior.

Observe that the KL divergence is the expectation of the log-density mismatch  $\log p(z|x) - \log p_\psi(z)$  with respect to the variational distribution  $p_\psi(z)$ . This means that the KL divergence places great importance on the log-density mismatch in the high-probability region of  $p_\psi(z)$ . A potential issue with standard VI stems from this property. Maximizing the ELBO—equivalently minimising the KL divergence—does not enforce the variational distribution  $q_\psi(z|x)$  to accurately estimate the tail probability of the posterior  $p(z|x)$ . It often prioritises finding one high-probability mode of a potentially multimodal posterior  $p(z|x)$ , leading to underestimation of the posterior variance. This motivates the development of more advanced objectives in VI, which will be discussed in Section 2.2.

VI is not limited to the case where the latent variable  $z$  is the model parameter. Some models, such as state-space models and generative models, have a separate model parameter  $\theta$  on top of the latent variable  $z$ . For example, variational autoencoders consist of encoder and decoder neural networks parametrised by  $\theta$ . They define a joint probability  $p(x, z | \theta)$  over data  $x$  and the encoder output  $z$ , conditional on the parameter  $\theta$ . Ideally, the model parameter  $\theta$  is optimised through maximisation of the marginal log likelihood  $\log p(x | \theta)$ . However, the marginal log likelihood  $\log p(x | \theta)$  is not computable. Alternatively, ELBO can be used as an approximation of the marginal log likelihood, where the model parameter  $\theta$  and the variational parameter  $\psi$  of the variational distribution over  $z$  are jointly optimised. We do not consider this setting in this paper. Still, our analysis, on the Wasserstein gradient and SNR, holds regardless of the conditional dependency of  $p(x, z)$  to the additional parameter  $\theta$ .

## 2.2 Importance-Weighted Evidence Lower Bound

The IW-ELBO was introduced in Burda et al. (2016) as an attempt to address the inherent limitations of the standard ELBO. Originally, Burda et al. (2016) used the terminology importance-weighted autoencoder (IWAE), since their focus was on training of variational autoencoders. Yet, their VI framework is generally applicable for any model, for which Domke and Sheldon (2018) coined the terminology, IW-ELBO, adapted in this paper. The IW-ELBO does not affect the choice of the variational distribution in VI; given a variational distribution of choice, it offers a tighter lower bound of the log marginal likelihood than the standard ELBO.

The IW-ELBO leverages importance weights of samples from the variational distribution  $q_\psi(z)$  to construct an accurate estimate of the log-likelihood. Using  $K$  i.i.d. random variables  $z_1, \dots, z_K$  following  $q_\psi(z)$ , the IW-ELBO is defined as follows:

$$\text{IW-ELBO}_K(q_\psi) = \mathbb{E}_{z_1, \dots, z_K \stackrel{i.i.d.}{\sim} q_\psi} \left[ \log \left( \frac{1}{K} \sum_{k=1}^K \frac{p(x, z_k)}{q_\psi(z_k)} \right) \right]. \quad (1)$$

Notice that, when  $K = 1$ , the IW-ELBO coincides with the standard ELBO. The IW-ELBO interpolates between the ELBO and the marginal log-likelihood, monotonically in terms of the

sample number  $K$ . It follows from Jensen’s inequality (see e.g. (Burda et al., 2016)) that

$$\log p(x) \geq \text{IW-ELBO}_{K+1}(q_\psi) \geq \text{IW-ELBO}_K(q_\psi) \geq \text{ELBO}(q_\psi).$$

Furthermore, in the limit of the sample number  $K \rightarrow \infty$ , the IW-ELBO converges to the log marginal likelihood  $\log p(x)$  by the law of large numbers. This means that, given enough computational resources to draw a large number of samples, IW-ELBO can provide an arbitrarily accurate estimate of the log marginal likelihood. The superior performance of the IW-ELBO over the ELBO has been well documented in the literature (Burda et al., 2016; Mnih and Rezende, 2016; Tucker et al., 2019; Daudel et al., 2023).

To date, the optimisation of the variational parameter  $\psi$  through the IW-ELBO relies on standard stochastic gradient descent on the Euclidean space of  $\psi$ . This indicates the presence of the “objective-mechanism mismatch”. The objective in VI is intrinsically a functional over probability distributions. However, optimising it by standard gradient descent, as a function of the variational parameter  $\psi$ , ignores the differential structure of the space of probability distributions. A small update of the variational parameter  $\psi$  in the Euclidean space does not necessarily mean a reasonable update of the variational distribution itself. The trajectory of the optimisation, cast as the dynamics of the variational distribution, can be unstable and inefficient in such a case. The Wasserstein space, which we recap next, allows us to address the objective-mechanism mismatch in VI.

### 2.3 Wasserstein Geometry

The Wasserstein space is a metric space of probability distributions, equipped with the Wasserstein metric. The 2-Wasserstein metric between two measures  $\mu$  and  $\nu$  in  $\mathcal{P}_2(\mathbb{R}^d)$  is defined as

$$W_2(\mu, \nu) := \left\{ \inf_{T: T_\# \mu = \nu} \int_{\mathbb{R}^d} \|x - T(x)\|^2 \mu(dx) \right\}^{1/2}. \quad (2)$$

A map, denoted  $T_\mu^\nu$ , which attains the infimum in (2) is called the optimal transform map from  $\mu$  to  $\nu$ . The existence and uniqueness of the optimal map are well studied (Ambrosio et al., 2005; Villani, 2009). In fact, it exists and is unique whenever  $\mu$  admits a density. The Wasserstein metric induces a rich differential structure, which turns the space of probability distributions into a (weak) Riemmanian manifold.

**Riemmanian Structure.** Denote by  $\mathbb{W}_2(\mathbb{R}^d)$  the Wasserstein space under the 2-Wasserstein metric. Denote by  $L_\mu^2(\mathbb{R}^d)$  the space of measurable maps  $\xi : \mathbb{R}^d \rightarrow \mathbb{R}^d$ , s.t.,  $\int \|\xi(x)\|^2 \mu(dx) < \infty$ , with the inner product  $\langle \xi_1, \xi_2 \rangle_\mu = \int \langle \xi_1(x), \xi_2(x) \rangle \mu(dx)$ . In order to view the set  $\mathbb{W}_2(\mathbb{R}^d)$  as a Riemmanian manifold, the tangent space at each member  $\mu \in \mathbb{W}_2(\mathbb{R}^d)$  needs to be specified. It is established that the tangent space at each distribution  $\mu$  can be identified as

$$\mathcal{T}_\mu \mathbb{W}_2(\mathbb{R}^d) := \overline{\{\xi = \lambda(T_\mu^\nu - \text{Id}) \mid \nu \in \mathbb{W}_2(\mathbb{R}^d), \lambda > 0\}}^{L_\mu^2(\mathbb{R}^d)}$$

where the closure is taken with respect to  $L_\mu^2(\mathbb{R}^d)$ ; see e.g. (Ambrosio et al., 2005, Chapter 8). Then, the Wasserstein space  $\mathbb{W}_2(\mathbb{R}^d)$  forms a Riemannian manifold, together with the inner-product  $\langle \cdot, \cdot \rangle_\mu$  equipped on the tangent space  $\mathcal{T}_\mu \mathbb{W}_2(\mathbb{R}^d)$  at each  $\mu$  (Villani, 2009). The implication is significant: key concepts in calculus, such as gradient, geodesic convexity, and smoothness, can be extended to the space of probability distributions.

**Wasserstein Gradient.** Now, we review the notion of the Wasserstein gradient of a functional  $\mathcal{F}$  on  $\mathbb{W}_2(\mathbb{R}^d)$ . There exist several ways to define the Wasserstein gradient of  $\mathcal{F}$ ; a common way is to use the *first variation* (Santambrogio, 2015). The first variation of  $\mathcal{F}$  at a probability distribution  $\mu$  is a function  $\delta\mathcal{F}(\mu)/\delta\mu : \mathbb{R}^d \rightarrow \mathbb{R}$  satisfying

$$\lim_{\epsilon \rightarrow 0^+} \frac{\mathcal{F}(\mu + \epsilon\nu) - \mathcal{F}(\mu)}{\epsilon} = \int_{\mathbb{R}^d} \frac{\delta\mathcal{F}(\mu)}{\delta\mu}(x)\nu(dx) \quad (3)$$

for all signed measure  $\nu$ , s.t.  $\mu + \epsilon\nu \in \mathcal{P}_2(\mathbb{R}^d)$  holds for  $\epsilon > 0$  sufficiently small. Then, the Wasserstein gradient is a map  $\nabla^W\mathcal{F}(\mu) : \mathbb{R}^d \rightarrow \mathbb{R}^d$  defined as the (Euclidean) gradient of the first variation:

$$[\nabla^W\mathcal{F}(\mu)](x) = \nabla_x \frac{\delta\mathcal{F}(\mu)}{\delta\mu}(x).$$

We refer readers to Ambrosio et al. (2005) for full detail. The functional  $\mathcal{F}$  is said to be differentiable at  $\mu$  if the Wasserstein gradient  $\nabla^W\mathcal{F}(\mu)$  exists. The Wasserstein gradient can be interpreted as a direction in which the functional  $\mathcal{F}$  increases the most under the geometry of  $\mathbb{W}_2(\mathbb{R}^d)$ .

## 2.4 Bures-Wasserstein Geometry

Albeit the elegant theory, performing optimisation in the Wasserstein space can be computationally challenging in practice. Some quantities, such as the Wasserstein gradient, can be challenging to compute, even for commonly-used functionals  $\mathcal{F}$  like the KL divergence. Limiting ourselves to the space of Gaussian distributions has a major advantage in that most of the computations become tractable.

**Riemmanian Structure.** The space of non-degenerate Gaussian distributions, equipped with the Wasserstein distance, is called the *BW space* (Lambert et al., 2024) and denote  $\text{BW}(\mathbb{R}^d)$ . The BW space turns the space of Gaussian distributions into a Riemannian submanifold of  $\mathbb{W}_2(\mathbb{R}^d)$ , in which many calculus tools become more intuitive and efficiently implementable than that of  $\mathbb{W}_2(\mathbb{R}^d)$ . The tangent space of  $\text{BW}(\mathbb{R}^d)$ , at a Gaussian measure  $q = \mathcal{N}(m, \Sigma)$ , is identified as a set of affine maps

$$\mathcal{T}_q \text{BW}(\mathbb{R}^d) := \left\{ x \mapsto a + S(x - m) \mid a \in \mathbb{R}^d, S \in \mathcal{S}^d \right\},$$

as established in Diao et al. (2023). Given some  $a$  and  $S$ , the constant-speed curve  $q_t = \mathcal{N}(m_t, \Sigma_t)$  in the BW space, starting from  $q_0 = \mathcal{N}(m_0, \Sigma_0)$  along the tangent vector  $x \mapsto a + S(x - m_0)$ , can be expressed as  $q_t = \mathcal{N}(m_0 + ta, (tS + I)\Sigma_0(tS + I))$ . This curve is characterised by the evolution of the associated mean vector  $m_t$  and covariance matrix  $\Sigma_t$  s.t.

$$\frac{d}{dt}m_t = a \quad \text{and} \quad \frac{d}{dt}\Sigma_t = S\Sigma_0 + \Sigma_0S.$$

Therefore, the BW space enables us to describe the dynamics of Gaussian distributions in terms of both the distribution and parameter simultaneously. See Diao et al. (2023) for more detail.

**Bures-Wasserstein Gradient.** Since  $\text{BW}(\mathbb{R}^d)$  is an embedded submanifold of  $\mathbb{W}_2(\mathbb{R}^d)$ , the Riemmanian gradient of a functional  $\mathcal{F}$  on  $\text{BW}(\mathbb{R}^d)$  can be computed by projecting the Wasserstein gradient of  $\mathcal{F}$  onto the tangent space of  $\text{BW}(\mathbb{R}^d)$  (Lambert et al., 2024). The projected Wasserstein gradient is referred to as the *BW gradient*. It is derived, at each  $q = \mathcal{N}(m, \Sigma)$ , by

$$\nabla^{\text{BW}}\mathcal{F}(q) := \arg \min_{v \in \mathcal{T}_q \text{BW}(\mathbb{R}^d)} \|v - \nabla^W\mathcal{F}(q)\|_{L_q^2(\mathbb{R}^d)}.$$

Since the BW gradient is an element of the affine-function space  $\mathcal{T}_q \text{BW}(\mathbb{R}^d)$ , it can be expressed in the form of an affine map  $[\nabla^{\text{BW}} \mathcal{F}(q)](x) = a_* + S_*(x - m)$  with

$$a_* := \mathbb{E}_{X \sim q}[G(X)] \quad \text{and} \quad S_* := \mathbb{E}_{X \sim q}[\nabla G(X)], \quad (4)$$

where  $G : \mathbb{R}^d \rightarrow \mathbb{R}^d$  denotes the Wasserstein gradient  $[\nabla^W \mathcal{F}(q)](\cdot)$ .

### 3 Bures-Wasserstein Importance-Weighted Evidence Lower Bound

This section presents our main results concerning the IW-ELBO objective for Gaussian VI under the Wasserstein geometry. First, Section 3.1 derives the Wasserstein gradient of the IW-ELBO formulated as a functional on the Wasserstein space. Section 3.2 establishes the growth rate of its SNR with respect to  $K$ . Subsequently, Section 3.3 derives the BW gradient of the IW-ELBO and develops an efficient optimisation algorithm of the IW-ELBO on the BW space. Finally, Section 3.4 discusses the mass-covering property of the IW-ELBO on the BW space. Proofs of the technical results presented in this section are provided in the Appendix, unless otherwise stated.

#### 3.1 Wasserstein Gradient of IW-ELBO

We begin by providing a rigorous derivation of the Wasserstein gradient for the IW-ELBO. Recall that the Wasserstein gradient is defined over functionals of probability distributions. To this end, we reformulate the IW-ELBO as a functional of  $K$  probability distributions  $q_1, \dots, q_K$ :

$$\text{IW-ELBO}_K(q_1, \dots, q_K) := \mathbb{E}_{z_1 \sim q_1, \dots, z_K \sim q_K} \left[ \log \left( \frac{1}{K} \sum_{i=1}^K \frac{p(x, z_i)}{q_i(z_i)} \right) \right].$$

The standard IW-ELBO is recovered by substituting a parametric variational distribution  $q_\psi$  for all the  $K$  arguments  $q_1, \dots, q_K$ . In contrast, we consider a configuration where all  $K$  arguments  $q_1, \dots, q_K$  are set to a common arbitrary distribution  $q$ . For an arbitrary index  $n$ , fixing the  $K - 1$  arguments  $\{q_i\}_{i \neq n}$  to the common distribution  $q$ , we define a functional  $\mathcal{F}_n(q_n)$  on  $\mathbb{W}_2(\mathbb{R}^d)$  by

$$\mathcal{F}_n(q_n) := \mathbb{E}_{z_n \sim q_n} \left[ \mathbb{E}_{\{z_1, \dots, z_K\} \setminus z_n \stackrel{i.i.d.}{\sim} q} \log \left( \frac{1}{K} \frac{p(x, z_n)}{q_n(z_n)} + \frac{1}{K} \sum_{i \neq n} \frac{p(x, z_i)}{q(z_i)} \right) \right],$$

where the subscript  $\{z_1, \dots, z_K\} \setminus z_n \stackrel{i.i.d.}{\sim} q$  denotes that the variables  $\{z_i\}_{i \neq n}$  are i.i.d. random variables following  $q$ . This expression represents the IW-ELBO viewed as a functional of the  $n$ -th argument  $q_n$ . Our objective is to derive the Wasserstein gradient of the IW-ELBO with respect to  $q_n$ , demonstrating that the functional form of this gradient is identical for any index  $n$ .

**Proposition 1.** *Suppose standard conditions that allow interchanging derivative and expectation, the Wasserstein gradient of  $\mathcal{F}_n(q_n)$  at  $q_n = q$  is given by*

$$\nabla^W [\mathcal{F}_n(q)](z_n) = \mathbb{E}_{\{z_1, \dots, z_K\} \setminus z_n \stackrel{i.i.d.}{\sim} q} \left[ \left( \frac{w(z_n)}{\sum_{i=1}^K w(z_i)} \right)^2 \nabla_{z_n} \log w(z_n) \right] \in \mathbb{R}^d, \quad (5)$$

where we define  $w(z) := p(x, z)/q(z)$  for notational convenience.

The expression for the Wasserstein gradient (5) is invariant with respect to the index  $n$ , as (i) the weight function  $w$  is independent of  $n$ , and (ii) the expectation is invariant under permutations of the i.i.d. variables  $\{z_i\}_{i \neq n}$ . Note that  $z_n$  represents the location where the gradient is evaluated, where the subscript  $n$  serves merely as a notational placeholder. Consequently, without loss of generality, we can focus on the case  $n = K$ , yielding

$$\nabla^W [\mathcal{F}_K(q)](z) = \mathbb{E}_{z_1, \dots, z_{K-1} \stackrel{i.i.d.}{\sim} q} \left[ \left( \frac{w(z)}{\sum_{i=1}^{K-1} w(z_i) + w(z)} \right)^2 \nabla_z \log w(z) \right] \in \mathbb{R}^d. \quad (6)$$

This invariance implies that aggregating the Wasserstein gradients across different indices  $n$  is unnecessary. Indeed, any aggregation, such as the maximum, minimum, or average over  $n$ , reduces to the expression in (6), as the gradients are identical for all  $n$ .

When  $K = 1$ , the Wasserstein gradient (6) reduces to the well-known expression of the Wasserstein gradient of the ELBO, that is,  $\nabla^W [\text{ELBO}(q)](z) = \nabla_z \log w(z)$ . When  $K > 1$ , this Wasserstein gradient scales proportionally to the importance weight  $w(z)$ , relative to the other  $K - 1$  importance weights.

### 3.2 Signal-to-Noise Ratio of Wasserstein Gradient of IW-ELBO

As  $K$  increases, the IW-ELBO provides an arbitrarily tight lower bound of the marginal likelihood. However, while tighter bounds are generally desirable, Rainforth et al. (2018) observed that this tightness can hinder the optimisation of the variational parameters  $\psi$  in parametric VI. Consider the IW-ELBO (1) defined for a variational family  $q_\psi$  equipped with an  $s$ -dimensional parameter vector  $\psi = (\psi_1, \dots, \psi_s)$ . Assume that the variational family  $q_\psi$  can be expressed as the push-forward of a base noise distribution  $q_\epsilon$  under a differentiable transformation  $T_\psi$  parameterised by  $\psi$ . With this reparameterisation, the gradient of the IW-ELBO with respect to the  $r$ -th coordinate  $\psi_r$  is given by

$$\frac{\partial}{\partial \psi_r} \text{IW-ELBO}_K(q_\psi) = \mathbb{E}_{\epsilon_i \stackrel{i.i.d.}{\sim} q_\epsilon(\cdot)} \left[ \sum_{i=1}^K \frac{w_\psi(T_\psi(\epsilon_i))}{\sum_{k=1}^K w_\psi(T_\psi(\epsilon_k))} \frac{\partial}{\partial \psi_r} \log w_\psi(T_\psi(\epsilon_i)) \right], \quad (7)$$

where we denote  $w_\psi(z) = p(x, z)/q_\psi(z)$  for notational convenience. Let  $g_{M,K}^r(\psi)$  denote the Monte Carlo estimator of the gradient (7) constructed from  $M$  independent samples of the  $K$  variables  $\epsilon_1, \dots, \epsilon_K$ . Rainforth et al. (2018) showed that the SNR of this estimator scales as  $O(\sqrt{M}/\sqrt{K})$ :

$$\text{SNR}(g_{M,K}^r(\psi)) = \frac{|\mathbb{E}(g_{M,K}^r(\psi))|}{\sqrt{\mathbb{V}(g_{M,K}^r(\psi))}} = O(\sqrt{M}/\sqrt{K}).$$

As  $K$  increases, the SNR vanishes, implying that the relative variance of the Monte Carlo estimator with respect to the magnitude of the exact gradient diverges to infinity. This suggests that accurate estimation of the gradient (7) becomes increasingly challenging for large  $K$ .

The Wasserstein gradient (6) of the IW-ELBO features a squared normalized importance weight term  $(w(z)/\sum_{i=1}^{K-1} w(z_i) + w(z))^2$ , in contrast to the linear term appearing in the standard Euclidean gradient (7). This expression bears a close resemblance to the *doubly-reparameterized gradient* of the IW-ELBO, derived in Tucker et al. (2019). Tucker et al. (2019) demonstrated that the Monte Carlo

estimator for the doubly-reparameterised gradient exhibits an SNR scaling of  $O(\sqrt{MK})$ , effectively mitigating the deterioration observed in the standard gradient. Remarkably, the Wasserstein gradient (6) of the IW-ELBO exhibits this same favorable SNR scaling. This implies that the precision of the Wasserstein gradient estimator improves as  $K$  increases.

Consider a Monte Carlo estimator of the Wasserstein gradient (6), evaluated at an arbitrary location  $z$ , constructed from  $M$  independent samples of the  $K - 1$  variables  $z_1, \dots, z_{K-1}$ . The Wasserstein gradient (6) evaluated at  $z$  is a  $d$ -dimensional vector. Similarly to Rainforth et al. (2018), to facilitate our analysis, we consider the SNR of the  $i$ -th coordinate of the Wasserstein gradient. Let  $g_{M,K}^i(z)$  denote the  $i$ -th coordinate of this Monte Carlo estimator.

**Theorem 1.** *Assume that (i)  $\mathbb{E}_{Z \sim q}(w(Z)^4) < \infty$  and that (ii)  $\mathbb{E}_{Z \sim q}(w(Z)^{-12}) < \infty$ . Then, for any  $z$  at which  $w(z) > 0$ ,*

$$\text{SNR}(g_{M,K}^i(z)) = \Omega(\sqrt{MK}).$$

We emphasize that  $\text{SNR}(g_{M,K}^i(z))$  enjoys a *Big-Omega* rate of  $\sqrt{MK}$ . Hence, the SNR is strictly lower-bounded by a term that grows with  $K$ . This appealing property of the Wasserstein gradient estimator of IW-ELBO is empirically verified in Section 4.2.

### 3.3 Optimisation of the IW-ELBO on the BW Space

Practical optimisation algorithms of the standard ELBO on the BW space have been established in Lambert et al. (2024) and Diao et al. (2023). However, relying on the standard ELBO, these frameworks inherit the well-known limitation of underestimating the tails of the target density. To address this limitation, we develop an optimisation algorithm for the IW-ELBO within the BW geometry. We call our algorithm the *Bures-Wasserstein Importance-Weighted ELBO (BW-IW-ELBO)* VI. Rather than treating the IW-ELBO as a function over the Euclidean space of variational parameters  $(m, \Sigma)$ , we formulate it as a functional over the BW manifold of Gaussian distributions  $\mathcal{N}(m, \Sigma)$ . This perspective naturally lifts the optimisation problem from the Euclidean geometry to the Wasserstein geometry, shifting the focus from parameter estimation to distributional optimisation. As demonstrated in Section 3.2, this geometric reframing enables more efficient optimisation compared to standard Euclidean approaches.

To align with standard conventions in WGF, we focus on the minimisation of the *negative* IW-ELBO, which is equivalent to maximising the original objective. Building upon the derivation of the Wasserstein gradient, we now derive the BW gradient for the negative IW-ELBO. To this end, we first substitute a Gaussian distribution  $\mathcal{N}(m, \Sigma)$  for the argument  $q$  of the Wasserstein gradient (6). We then take a projection of the resulting Wasserstein gradient (6) onto the tangent space of the BW space, yielding the following proposition.

**Proposition 2.** *Under the same condition as Proposition 1, the BW gradient of the negative IW-ELBO,  $-\mathcal{F}_K(q)$ , at a Gaussian density  $q = \mathcal{N}(m, \Sigma)$  is given by*

$$\nabla^{\text{BW}}[-\mathcal{F}_K(q)](z) = a_* + S_*(z - m),$$

---

**Algorithm 1:** Bures-Wasserstein IW-ELBO method

---

**Input:** target density  $p$ , learning rate  $\eta$ .  
**Output:** A Gaussian distribution that approximates the target  $p$ .  
 Initialise the mean and covariance parameters  $m, \Sigma$   
**while** *not stop* **do**  
 | compute Monte Carlo estimates  $\hat{a}_*$  and  $\hat{S}_*$  from (8) and (9)  
 | Update  $m \leftarrow m - \eta \hat{a}_*$   
 | Update  $\Sigma \leftarrow (I - \eta \hat{S}_*) \Sigma (I - \eta \hat{S}_*)$ .  
**end**

---

where the vector  $a_*$  and the matrix  $S_*$  are defined as, respectively,

$$a_* := - \mathbb{E}_{z_1, \dots, z_K \stackrel{i.i.d.}{\sim} \mathcal{N}(m, \Sigma)} \left[ \left( \frac{w(z_K)}{\sum_{i=1}^K w(z_i)} \right)^2 \nabla_{z_K} \log w(z_K) \right]; \quad (8)$$

$$S_* := - \mathbb{E}_{z_1, \dots, z_K \stackrel{i.i.d.}{\sim} \mathcal{N}(m, \Sigma)} \left[ \nabla_{z_K} \left\{ \left( \frac{w(z_K)}{\sum_{i=1}^K w(z_i)} \right)^2 \nabla_{z_K} \log w(z_K) \right\} \right]. \quad (9)$$

Here, the weight function  $w(z) = p(x, z)/q(z)$  is defined with the Gaussian density  $q = \mathcal{N}(m, \Sigma)$ .

*Proof.* The proof is a direct implication of (4) and (6).  $\square$

The BW gradient represents the steepest descent direction of the negative IW-ELBO at the given density  $q = \mathcal{N}(m, \Sigma)$  with respect to the BW geometry.

We now formulate the gradient descent scheme for minimising the negative IW-ELBO on the BW manifold. Let  $q^{(k)} = \mathcal{N}(m_k, \Sigma_k)$  denote the iterate at step  $k$ , initialised at  $q^{(0)} = \mathcal{N}(m_0, \Sigma_0)$ . Adopting the standard discretisation scheme for WGF (e.g. Ambrosio et al., 2005), we update the Gaussian density  $q^{(k)}$  at step  $k$  via the following push-forward operation:

$$q^{(k+1)} = (\text{Id} - \eta \nabla^{\text{BW}} \mathcal{F}_1(q^{(k)}))_{\#} q^{(k)} \quad (10)$$

where  $\eta$  denotes the step size of the update. Remarkably, since the push-forward map is affine, the update in (10) corresponds to the following updates for the associated mean and covariance:

$$m_{k+1} = m_k - \eta a_* \quad \text{and} \quad \Sigma_{k+1} = (I - \eta S_*) \Sigma_k (I - \eta S_*).$$

The complete procedure is summarised in Algorithm 1.

In contrast to the forward-backward approach of Diao et al. (2023) designed for optimising the ELBO, our approach omits the backward step. While the backward step is required to ensure convergence due to the non-smoothness of the entropy term in the ELBO, it imposes a substantial computational burden. Crucially, the negative IW-ELBO does not admit the decomposition into a convex potential and a non-smooth entropy term exploited in Diao et al. (2023). Moreover, as the smoothness properties of this objective remain ambiguous, the theoretical necessity of the backward step is indeterminate. We leave the rigorous analysis of this theoretical aspect to future research.

### 3.4 Mass Covering Property of BW-IW-ELBO

Maximizing the ELBO objective is equivalent to minimizing the KL divergence

$$\text{KL}(q\|p) = \int_Z q(z) \log \frac{q(z)}{p(z|x)} dz$$

from the variational approximation  $q(z)$  to the posterior  $p(z|x)$ , typically referred to as the reverse KL divergence. A critical property of this formulation is that the divergence diverges to infinity if  $q(z)$  assigns non-zero probability to regions where  $p(z|x)$  is zero. Consequently, to maintain a finite objective, the optimisation process implicitly constrains the support of  $q(z)$  to lie within the support of  $p(z|x)$ . This constraint has significant practical implications, primarily inducing the ‘mode-seeking’ or ‘zero-forcing’ behaviour in the variational approximation (Li and Turner, 2016). When the posterior distribution is multimodal, minimising this divergence typically results in  $q(z)$  concentrating on a single mode, assigning negligible probability mass to other modes; see an empirical illustration of this behaviour in Section 4. While the resulting approximation  $q(z)$  may provide an accurate local representation of a single mode, it often fails to capture the global structure of the true posterior, leading to severe variance underestimation and an inability to represent multimodality.

To alleviate the mode-seeking behavior of the standard ELBO, the IW-ELBO provides a tighter lower bound on the log marginal likelihood using the  $K$  multiple random variables. This bound becomes strictly tighter as  $K \rightarrow \infty$ , converging monotonically to the log marginal likelihood. Maximising this IW-ELBO has been shown to be equivalent to minimising the KL divergence defined on an augmented sample space of the multiple random variables (Cremer et al., 2017; Domke and Sheldon, 2018). Tan et al. (2020) demonstrated that the IW-ELBO admits an asymptotic expansion

$$\text{IW-ELBO}_K(q) \approx \log p(x) - \frac{\mathbb{V}_{Z \sim q}(w(Z))}{K p(x)}.$$

This expansion implies that maximising the IW-ELBO effectively minimises the variance of the importance weight  $\mathbb{V}_{Z \sim q}(w(Z))$ . This penalises variational approximations  $q$  that possess lighter tails than the posterior  $p(z|x)$ , promoting the mass-covering property characteristic of the IW-ELBO methods. As a consequence, the IW-ELBO constitutes a statistically powerful objective for approximating complex and multi-modal posteriors.

The BW-IW-ELBO method inherits the mass-covering property from the IW-ELBO objective, while the optimisation is conducted on the BW manifold, exploiting its rich geometric structure. This synergy offers a distinct advantage. The IW-ELBO objective drives the variational density  $q$  to cover the posterior mass, and the BW geometry dictates the optimal trajectory for this evolution. For example, in the case of a bimodal posterior, the IW-ELBO objective encourages expansion of the support of  $q$  to cover both the modes, while the BW geometry facilitates efficient covariance updates for the density  $q$  to have such a support. In contrast, standard parametric IW-ELBO methods perform updates within the Euclidean space of the variational parameter. The flat geometry of this space fails to capture the intrinsic geometry of the variational distributions, often resulting in suboptimal optimisation trajectories and slower convergence.

## 4 Numerical Examples and Applications

We empirically assess the performance of the BW-IW-ELBO method by two experiments presented in this section. Section 4.1 focuses on approximation of a synthetic yet challenging density, called the *eggbox* distribution, which is highly multimodal. Section 4.2 addresses a real-world application of Bayesian logistic regression, where the posterior is efficiently approximated by our proposed method.

### 4.1 Eggbox distributions

#### BW-IW-ELBO for target approximation

We conduct an empirical study to demonstrate the mass-covering property of BW-IW-ELBO where the task is to approximate the eggbox distribution (Murray et al., 2010) - a multimodal distribution. The mass-covering property is critical in applications where the primary focus is on capturing uncertainty rather than point estimate. A mode-seeking approximation that collapses to a single mode might severely underestimate the true posterior uncertainty, leading to overconfident and unreliable predictions. In contrast, a mass-covering approximation spreads the mass to encompass all major modes, providing a more reliable and robust approximation.

Our experiment is conducted in a two-dimensional space where the target distribution has four equally-weighted Gaussian components (eggs=4). The task is to optimise the parameters (mean and covariance) of a single Gaussian distribution  $q$  to best approximate this target. We compare the performance of our BW-IW-ELBO with the black-box Mean-Field Variational Bayes (MFVB) Ranganath et al. (2014) and the baseline Forward-Backward Gaussian Variational Inference (FB-GVI) of Diao et al. (2023).

The optimisation process and approximation results are visualised in Figure 1. The ground truth four-egg target is shown with solid contours and the learned variational approximation  $q$  is shown with dashed contours. As the optimisation proceeds, the dashed contours shift and reshape from their initial configuration. As shown, the BW-IW-ELBO achieves the best mass-covering behavior as its final learned Gaussian becomes sufficiently elongated, with its contours stretching to encompass all four peaks of the true target distribution.

#### BW-IW-ELBO for an efficient importance distribution

Given the mass-covering property of BW-IW-ELBO, its Gaussian approximation can be useful in a downstream application, such as being used as a proposal distribution in importance sampling or MCMC.

Suppose that we want to estimate the mean and covariance matrix of the target four-egg distribution; we perform this task by importance sampling with a VI Gaussian approximation as an importance proposal. The mean and covariance of this equally-weighted eggbox distribution are given as

$$\mu_{\text{GMM}} = \frac{1}{4} \sum_{k=1}^4 \mu_k, \quad \Sigma_{\text{GMM}} = \frac{1}{4} \sum_{k=1}^4 \Sigma_k + \frac{1}{4} \sum_{k=1}^4 (\mu_k - \mu_{\text{GMM}})(\mu_k - \mu_{\text{GMM}})^\top$$

with  $\mu_k$ ,  $\Sigma_k$  the component means and component covariances. Using these analytical moments as the ground truth, we evaluated the accuracy of the importance sampling approximations. Table 1 reports the Mean Squared Error (MSE) for both the estimated mean and covariance, alongside

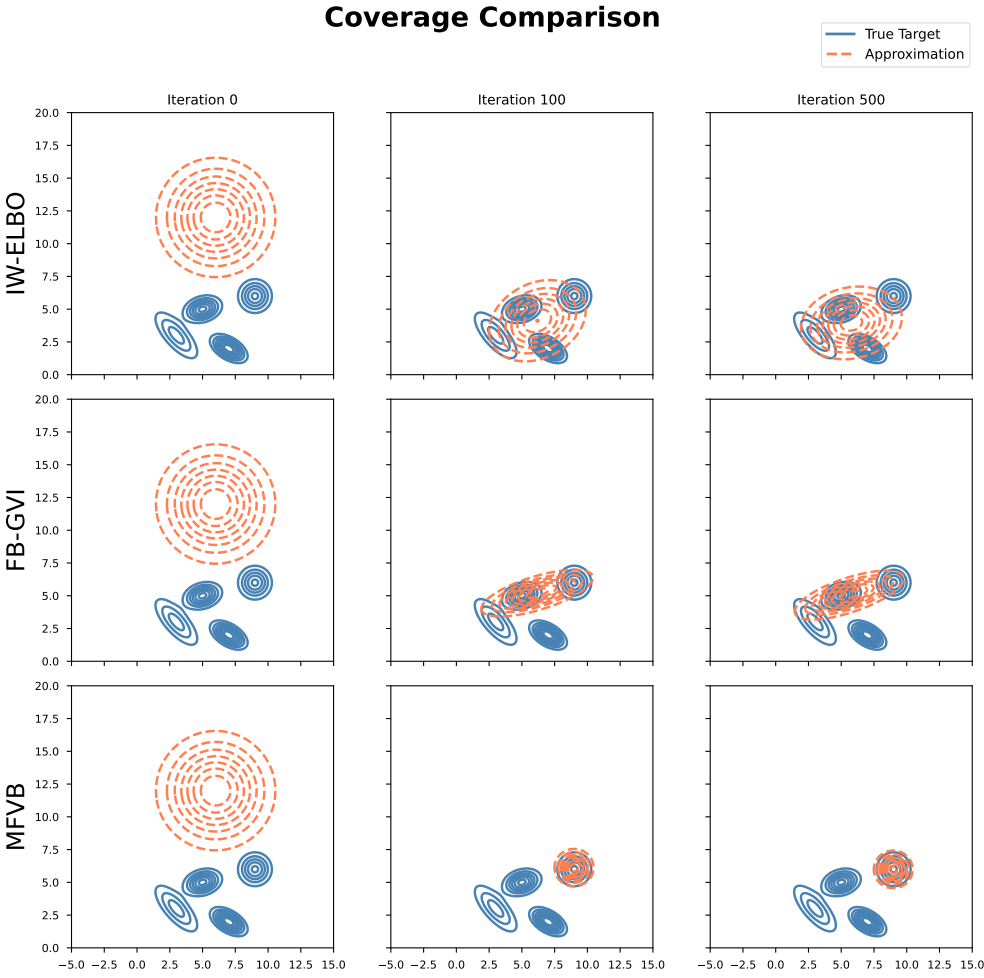


Figure 1: Evolution of the variational approximation for a four-peaked eggbox target. The BW-IW-ELBO is the only method that successfully learns a single Gaussian to cover all four modes of the true target distribution, demonstrating superior mass-covering behavior.

the final ELBO values. Our proposed BW-IW-ELBO approximation significantly outperforms the baselines (FB-GVI and MFVB), achieving smallest MSE on the moment parameters and the tightest lower bound. These quantitative results show that the BW-IW-ELBO approximation accurately captures the geometry of the target multimodal distribution, confirming its suitability as a reliable importance proposal distribution for downstream inference tasks.

## 4.2 Bayesian Logistic Regression

This section empirically examines the performance of the VI methods in the context of a Bayesian logistic regression model. We use the census data from the UCI Machine Learning Repository; the task is to predict an individual’s income level (greater than or equal to \$50,000) based on their attributes. To reduce the size and collinearity, the initial attributes are first pre-processed to reduce to 8 features using principal component analysis. The model assumes a Bernoulli distribution for

Table 1: Quantitative comparison of approximation fidelity. The reported numbers are summarised over multiple independent runs

Method	MSE(Mean) $\downarrow$	MSE(Cov) $\downarrow$	ELBO/IW-ELBO $\uparrow$
IW-ELBO	<b>0.0150</b>	<b>1.0026</b>	<b>-0.0011 <math>\pm</math> 0.0226</b>
FB-GVI	1.2338	6.3469	-0.2494 $\pm$ 0.1525
MFVB	12.8031	36.1071	-1.1964 $\pm$ 0.5472

the binary outcome  $y_i \in \{0, 1\}$  given a feature vector  $X_i$ :

$$p(y_i|X_i, \theta) = \text{Bernoulli}(\sigma(X_i^T \theta))$$

where  $\sigma(\cdot)$  is the sigmoid function and  $\theta$  is the vector of coefficients. We impose a standard  $L_2$  regularisation prior,  $\theta \sim \mathcal{N}(0, \sigma_0^2 I)$  with  $\sigma_0^2 = 10$ . The inference goal is to approximate the posterior distribution  $p(\theta|\mathcal{D})$  given the data  $\mathcal{D} = \{(X_i, y_i), i = 1, \dots, n\}$ .

### Evaluating the performance of gradient estimators

We examine the performance of the various gradient estimators within the context of maximising the IW-ELBO. The variational family is multivariate Gaussian distributions parameterised by a mean vector  $\mu$  and a covariance matrix  $\Sigma$ . To optimise the IW-ELBO in the Euclidean setting, we use the ADAM optimiser and represent the covariance via the Cholesky decomposition,  $\Sigma = LL^\top$ , with  $L$  a lower triangular matrix.

First, we compute the Monte Carlo estimate of the SNR of the Wasserstein gradient estimator (5), evaluated at a central value of  $\theta$ , for various  $K$ . As shown in Figure 2, when  $K$  increases from 10 to  $10^3$ , the SNR for each dimension keeps rising. This implies that, as predicted in Theorem 1, the Wasserstein gradient signal becomes stronger relatively to its variance when more samples are used. In stark contrast, for the standard Euclidean gradient estimator, the decrease of its SNR has been well documented in the literature (Rainforth et al., 2018; Daudel and Roueff, 2024).

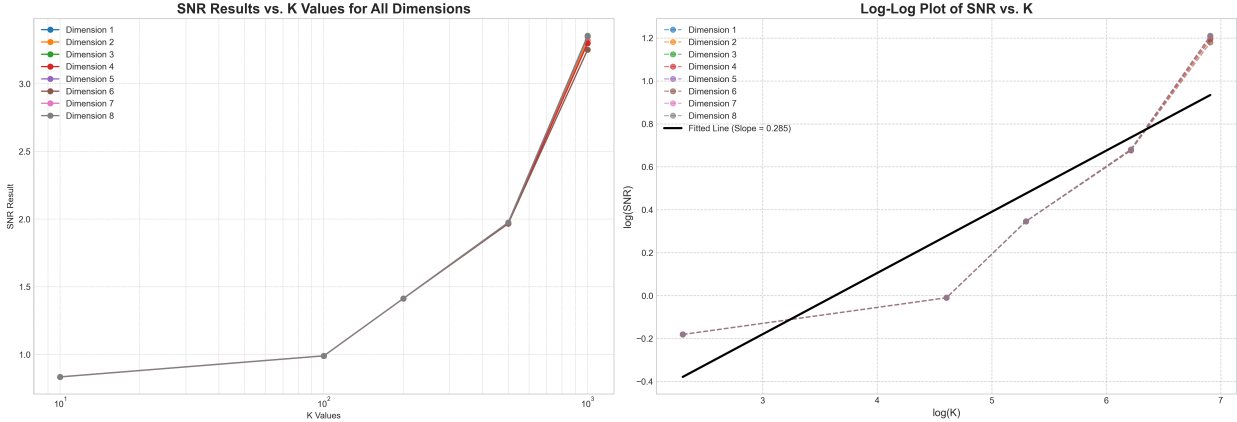


Figure 2: SNR of the Wasserstein gradient estimator v.s.  $K$  for all dimensions. The straight line is the fitted regression line.

Next, we examine the convergence dynamics of two methods for optimising the IW-ELBO bound: one using the Euclidean gradient with the ADAM optimiser, and the other using BW gradient. A clear pattern in Figure 3 emerges for the BW-IW-ELBO algorithm: the number of iterations needed to reach convergence steadily decreases as  $K$  increases. This indicates that the BW gradient effectively leverages the richer information from a larger sample set to accelerate optimisation. It is also much more stable as the variation across different runs (shown by the vertical bars) are small. Conversely, the convergence speed of the standard Euclidean gradient shows little dependence on  $K$ ; it is unstable with massive variance in its convergence time. This difference in behavior underscores a significant benefit of the BW gradient: it navigates the parameter space more efficiently when provided with more samples, resulting in faster and more stable convergence behavior.

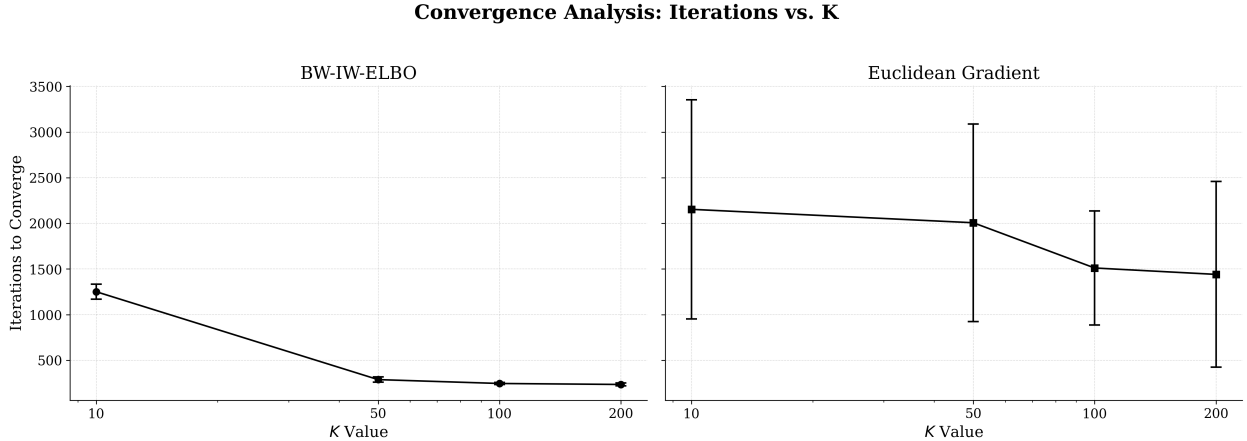


Figure 3: Number of iterations until convergence for various  $K$ . The vertical bars show the variation across different runs

Figure 4 depicts that the BW-IW-ELBO method consistently achieves a higher final IW-ELBO than the ADAM optimiser, irrespective of the number of importance samples  $K$ . A higher IW-ELBO corresponds to a tighter bound on the marginal log-likelihood, implying a more accurate posterior approximation. This enhanced accuracy is a primary advantage of our approach, leading to improved model fidelity and more dependable uncertainty estimates.

### Accuracy of posterior approximation

We now assess the performance of the BW-IW-ELBO method in terms of posterior approximation accuracy. For comparison, we implement a conventional Black-box VI approach (referred to as MFVB) that uses a fully factorized variational distribution:

$$q(\theta|\mu, \text{diag}(\sigma^2)) = \prod_{j=1}^d \mathcal{N}(\theta_j|\mu_j, \sigma_j^2).$$

We note that the BW-IW-ELBO method employs a more flexible variational family using a multivariate Gaussian with a full covariance matrix,  $q(\theta|\mu, \Sigma) = \mathcal{N}(\theta|\mu, \Sigma)$ . This richer distribution is capable of capturing the posterior dependencies between the parameters.

### Convergence Tracking Comparison

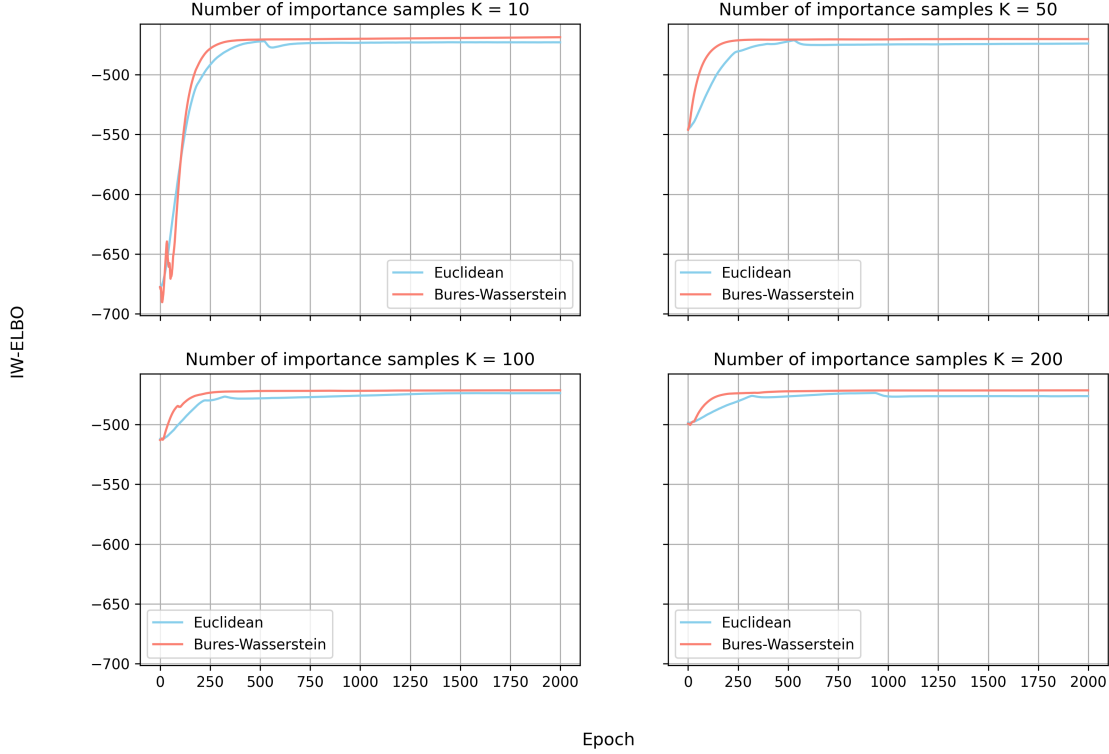


Figure 4: IW-ELBO bound estimates over iterations

To assess the quality of the final learned approximations, we use several metrics. The first is the ELBO estimated using Monte Carlo samples from  $q(\theta)$ )

$$\widehat{\text{ELBO}}(q) = \frac{1}{M} \sum_{i=1}^M \left[ \log p(\mathcal{D}, \theta_i) - \log q(\theta_i) \right].$$

The second metric is Effective Sample Size (ESS)

$$\text{ESS} = \frac{(\sum_{i=1}^M w_i)^2}{\sum_{i=1}^M w_i^2},$$

where  $w_i = p(\mathcal{D}, \theta_i)/q(\theta_i)$  are the unnormalized importance weights. The ESS quantifies the efficiency of  $q$  when used as an importance distribution; the higher the better. Finally, we conduct a qualitative analysis by comparing both variational distributions against a high-fidelity ground truth approximation based on a long-run MCMC simulation.

The quantitative results, summarised in Table 2, demonstrate that our BW-IW-ELBO approach (using the full-covariance  $q$ ) achieves a superior ELBO and ESS compared to the MFVB baseline. This quantitative superiority is corroborated by the qualitative comparison in Figure 5, which presents pairwise contours together with one-dimensional marginals for the posterior of several

Table 2: Performance comparison for census data: ESS and ELBO are evaluated based on 10000 samples. These numbers are averaged over 100 running times.

Method	ESS $\uparrow$	IW-ELBO $\uparrow$
BW-IW-ELBO	<b>9963.99 <math>\pm</math> 1.11</b>	<b>-15753.71 <math>\pm</math> 0.001</b>
MFVB	311.58 $\pm$ 210.32	-15755.14 $\pm$ 0.021

selected parameters, estimated by MFVB, BW-IW-ELBO and MCMC. In the marginal posterior plots, while both the MFVB and BW-IW-ELBO approximations successfully capture the mode of the true posterior, the shape (i.e., width and height) of the BW-IW-ELBO approximation provides a visibly closer match to the MCMC ground truth. The limitations of the mean-field assumption become starkly apparent in the two-dimensional joint posterior contours. The MCMC samples form tilted ellipses, indicating significant posterior correlation between pairs of parameters. The MFVB contours, constrained by the factorized assumption, are necessarily aligned with the plot axes and are structurally incapable of capturing this correlation. In sharp contrast, the contours from our IW-ELBO method (orange contour) are also tilted ellipses and closely align with the MCMC ground truth in both shape and orientation. This visually confirms that the full-covariance model, trained with our BW-IW-ELBO algorithm, successfully learns and represents better coverage.

In summary, both quantitative metrics and visual inspection against an MCMC baseline confirm that the full-covariance approximation trained with the BW-IW-ELBO algorithm yields a more accurate and faithful representation of the true posterior distribution than the standard mean-field approach. Its ability to model covariance is essential for this problem.

## 5 Extension to Bures-Wasserstein VR-IWAE

This section explores the connections between our BW-IW-ELBO framework and the VR-IWAE bound. The VR-IWAE bound represents another emerging objective function for VI, sharing key properties with the IW-ELBO. While the primary focus of this work is investigating the desirable properties of the BW-IW-ELBO and developing the corresponding optimisation algorithm, the majority of the results presented in Section 3 extend readily to the VR-IWAE bound. Our empirical evaluation for the VR-IWAE bound is restricted to a proof-of-concept, given that a comprehensive analysis lies beyond the current scope of this work. Yet, it offers valuable insights into the potential for generalising the BW-IW-ELBO methods.

### 5.1 Variational Renyi Importance-Weighted Autoencoder Bound

First, we recap the formulation of the VR-IWAE bound. Daudel et al. (2023) derived the VR-IWAE bound by combining the Variational Renyi (VR) bound of Li and Turner (2016) with the IW-ELBO bound. Given a power hyperparameter  $\alpha \in [0, 1]$ , the VR-IWAE bound is expressed as follows:

$$\text{VR-IWAE}_K^{(\alpha)}(q_1, \dots, q_K) = \frac{1}{1 - \alpha} \mathbb{E}_{z_1 \sim q_1, \dots, z_K \sim q_K} \left[ \log \left( \frac{1}{K} \sum_{i=1}^K \frac{p(x, z_i)^{1-\alpha}}{q_i(z_i)^{1-\alpha}} \right) \right], \quad K \geq 1.$$

where each  $q_i$  is set to a common variational distribution  $q$ . The VR-IWAE bound coincides with the IW-ELBO when  $\alpha = 0$ , but it exhibits flexible bias-variance trade-off when  $\alpha > 0$  which allows

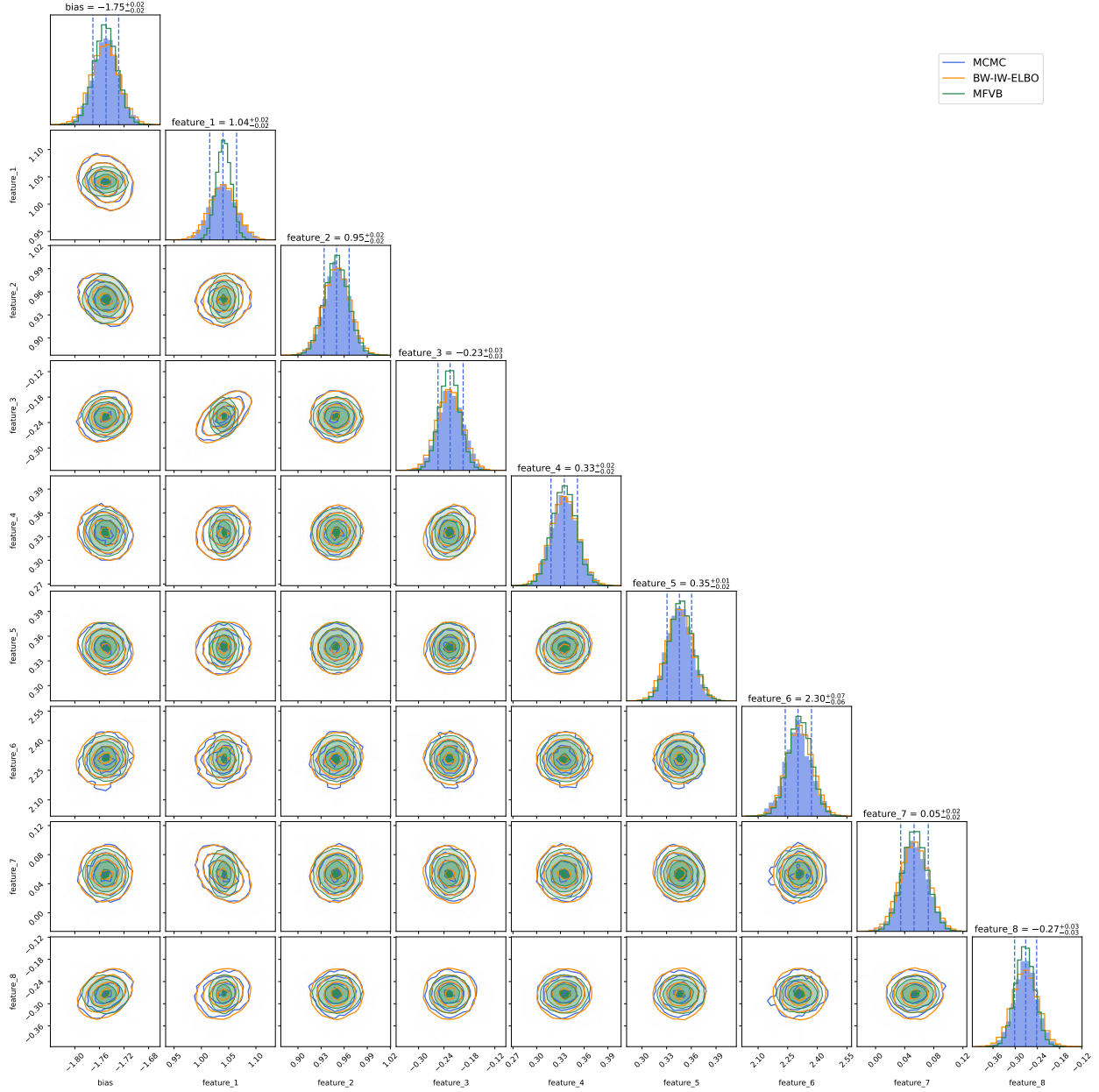


Figure 5: Pairwise and Marginal Posterior Comparisons

VI to be used more efficiently in challenging applications.

In standard parametric VI, the variational distribution  $q$  is set to a parametric family  $q_\psi$  equipped with the parameter vector  $\psi$ . A significant advantage of the VR-IWAE bound is that it admits an unbiased estimator of the Euclidean gradient with respect to  $\psi$ , in stark contrast to the VR bound. Another advantage is that the SNR of the Euclidean gradient of the VR-IWAE bound scales at the increasing rate  $O(\sqrt{K})$ , in contrast to the case of the IW-ELBO.

## 5.2 Wasserstein Gradient of the VR-IWAE Bound

Next, we extend our analysis of the Wasserstein gradient of the IW-ELBO to the VR-IWAE bound. Similarly to Section 3.1, we began by viewing the VR-IWAE bound as a functional over  $K$  probability distributions  $q_1, \dots, q_K$ . For an arbitrary index  $n$ , fixing the  $K - 1$  arguments  $\{q_i\}_{i \neq n}$  to the common distribution  $q$ , we define a functional  $\mathcal{G}_n(q_n)$  on  $\mathbb{W}_2(\mathbb{R}^d)$  by

$$\mathcal{G}_n(q_n) := \frac{1}{1 - \alpha} \mathbb{E}_{z_n \sim q_n} \left[ \mathbb{E}_{\{z_1, \dots, z_K\} \setminus z_n \stackrel{i.i.d.}{\sim} q} \log \left( \frac{1}{K} \frac{p(x, z_n)^{1-\alpha}}{q_n(z_n)^{1-\alpha}} + \frac{1}{K} \sum_{i \neq n} \frac{p(x, z_i)^{1-\alpha}}{q(z_i)^{1-\alpha}} \right) \right],$$

This expression represents the VR-IWAE bound viewed as a functional of the  $n$ -th argument  $q_n$ . Following Section 3.1, our objective is to derive the Wasserstein gradient of the VR-IWAE bound with respect to  $q_n$ , demonstrating that the form of this gradient is identical for any index  $n$ .

**Proposition 3.** *Suppose standard conditions that allow interchanging derivative and expectation. The Wasserstein gradient of the VR-IWAE bound  $\mathcal{G}_n(q_n)$  at  $q_n = q$  is given by*

$$\nabla^W [\mathcal{G}_n(q)] (z_n) = \mathbb{E}_{\{z_1, \dots, z_K\} \setminus z_n \stackrel{i.i.d.}{\sim} q} \left[ \left( \alpha \frac{w(z_n)^{1-\alpha}}{\sum_{i=1}^K w(z_i)^{1-\alpha}} + (1 - \alpha) \left( \frac{w(z_n)^{1-\alpha}}{\sum_{i=1}^K w(z_i)^{1-\alpha}} \right)^2 \right) \nabla_{z_n} \log w(z_n) \right] \in \mathbb{R}^d. \quad (11)$$

The proof is deferred to the Appendix. By the exactly same argument in Section 3.1, this expression for the Wasserstein gradient (11) is invariant with respect to the index  $n$ . Therefore, without loss of generality, we can focus on the case  $n = K$ .

Interestingly, the Wasserstein gradient (11) shares a similar form to the doubly-reparameterized gradient of the parametric VR-IWAE bound. Daudel and Roueff (2024) showed that the SNR of the doubly-reparameterized gradient estimator for the parametric VR-IWAE bound enjoys the increasing rate of  $O(\sqrt{K})$ . A Monte Carlo estimator of the Wasserstein gradient (11) of the VR-IWAE bound  $\mathcal{G}_K(q)$  also enjoys the same growth rate of the SNR. Let  $g_{\alpha, M, K}^r(z)$  be the  $r$ -th coordinate of the Monte Carlo estimator of the Wasserstein gradient (11) of  $\mathcal{G}_K(q)$ , evaluated at a location  $z$ , constructed from  $M$  independent samples of the  $K - 1$  variables  $z_1, \dots, z_{K-1}$ .

**Theorem 2.** *Let  $\alpha \in [0, 1)$  and assume that  $\mathbb{E}_{Z \sim q}(w(Z)^{4(1-\alpha)}) < \infty$  and  $\mathbb{E}_{Z \sim q}(w(Z)^{-12(1-\alpha)}) < \infty$ . Then, for any  $z_n$  with  $w_n(z_n) > 0$ ,*

$$SNR(g_{\alpha, M, K}^r(z_n)) = \Omega(\sqrt{MK}), \quad r = 1, \dots, d_z.$$

The proof is similar to that of Theorem 1 and hence omitted.

## 5.3 Optimisation of the VR-IWAE Bound on the BW Space

To align with standard conventions in WGF, we focus on the minimisation of the negative VR-IWAE bound, which is equivalent to maximising the original objective. To formulate the gradient descent scheme for minimising the negative IW-ELBO, we first derive the BW gradient for the negative VR-IWAE bound. For notational convenience, denote by  $G(z)$  the Wasserstein gradient (11) of

the VR-IWAE bound  $\mathcal{G}_K(q)$ , evaluated at  $z$ . Following the same derivation in Section 3.3, the BW gradient of the negative VR-IWAE bound  $-\mathcal{G}_K(q)$  at a Gaussian density  $q = \mathcal{N}(m, \Sigma)$  is given by

$$\nabla^{\text{BW}}[-\mathcal{G}_K(q)](z) = a_* + S_*(z - m),$$

where the vector  $a_*$  and matrix  $S_*$  are defined by, respectively,

$$a_* = -\mathbb{E}_{z_K \sim q}[G(z_K)], \quad \text{and} \quad S_* = -\mathbb{E}_{z_K \sim q}[\nabla G(z_K)]. \quad (12)$$

The explicit expressions for  $a_*$  and  $S_*$  and their Monte Carlo estimates can be found in the Appendix. Algorithm 1 presented in Section 3.3 is readily amenable to this BW gradient, by replacing the vector  $a_*$  and matrix  $S_*$  in Algorithm 1 with the above ones.

We assess the efficacy of the VI algorithm on a unimodal yet challenging toy density, often referred to as the banana-shaped distribution (Haario et al., 2001). Let  $q$  denote the density function of a  $d$ -dimensional Gaussian distribution  $\mathcal{N}(0, \Sigma)$  with the covariance  $\Sigma = \text{diag}(100, 1, \dots, 1)$ . Given a constant hyperparameter  $b > 0$ , this distribution is defined as  $\pi(x) = q(\phi(x))$ , where

$$\phi(x) = (x_1, x_2 + bx_1^2 - 100b, x_3, \dots, x_d) \in \mathbb{R}^d.$$

Despite its unimodality, this target poses a significant challenge for VI methods due to its highly non-Gaussian geometry characterized by extended, narrow tails. Varying the hyperparameter  $b$  adjusts the curvature, and hence the degree of non-Gaussianity (Haario et al., 2001), where we used  $b = 0.03$  in this experiment. We approximated this target density by a single multivariate Gaussian, comparing different VI algorithms initialized with an identical distribution. Figure 6 illustrates the outcome of each algorithm, visualising the contour plots of the evolving Gaussian approximations against the scatter plot of samples drawn from the true banana-shaped distribution. The true banana-shaped distribution cannot be exactly recovered by the Gaussian variational family. The algorithms exhibit distinct qualitative behaviours in their approximations. The FB-GVI algorithm of Diao et al. (2023) substantially underestimates the variance of the target, resulting in an excessively narrow approximation. In contrast, the BW-IW-ELBO method proposed in this work demonstrates superior performance in capturing the target's dispersion. The VR-IWAE method shares a similar performance to the BW-IW-ELBO method. The setting  $\alpha = 0.1$  yields the most accurate approximation, surpassing the performance of both  $\alpha = 0.5$  and  $\alpha = 0.9$ .

## 6 Conclusion

This work bridges the gap between two distinct paradigms, IW-ELBO in Importance Weighted VI and WGF in Optimal Transport, by casting the optimization of IW-ELBO as a problem defined on the Bures-Wasserstein space. This formulation revealed the advantageous scaling properties of the SNR associated with the Wasserstein gradient estimator for IW-ELBO. In turn, this elucidates the theoretical mechanisms rendering optimization in this geometric framework more stable and efficient than conventional Euclidean methods. Building upon this foundation, we introduced the BW-IW-ELBO algorithm, which enables a tractable optimization of the IW-ELBO of the Gaussian family under the Bures-Wasserstein geometry. We evaluated the resulting Gaussian approximations and demonstrated, via extensive numerical experiments, that BW-IW-ELBO exhibits both mass-covering behavior and high approximation accuracy, particularly in complex multimodal settings where standard Gaussian variational methods typically underperform.

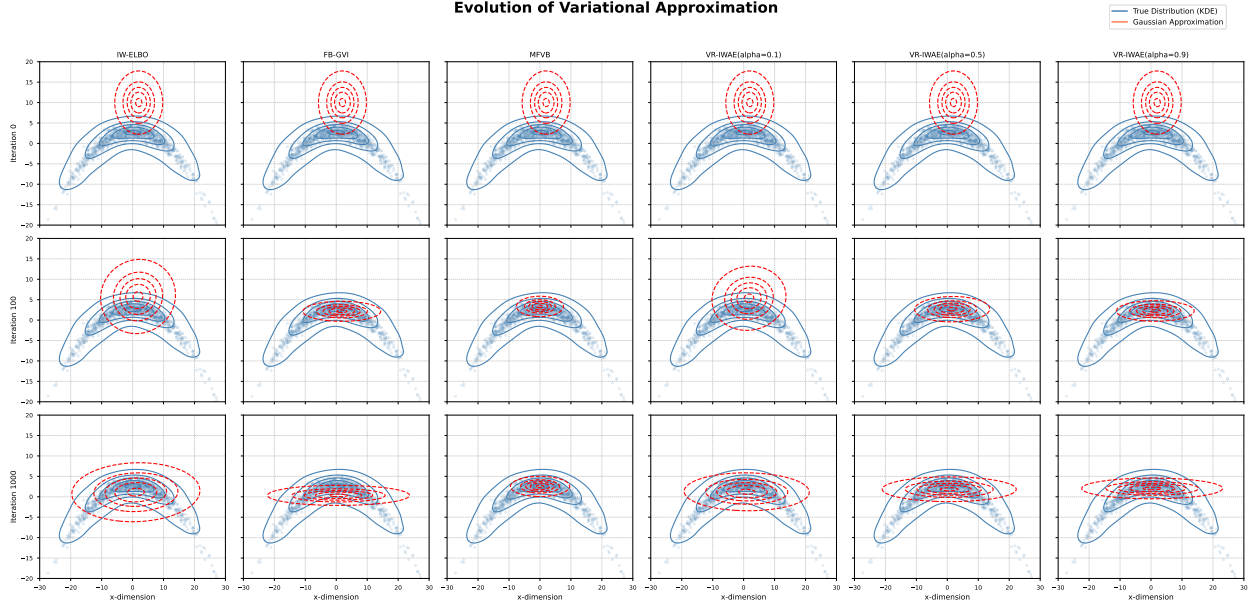


Figure 6: A comparison of different VI algorithms for banana-shaped distribution

Several promising avenues for future research remain. A rigorous theoretical analysis of the convergence properties of the BW-IW-ELBO algorithm remains to be established; providing such results would bolster the methodological foundation of our approach. Furthermore, extending IW-ELBO optimization to broader geometric spaces beyond the Bures–Wasserstein manifold may yield even more robust variational frameworks and a deeper understanding of the interplay between optimal transport geometry and importance-weighted variational inference.

## References

- Ambrosio, L., Gigli, N., and Savaré, G. (2005). *Gradient Flows In Metric Spaces and in the Space of Probability Measures*. Birkhäuser Basel.
- Burda, Y., Grosse, R., and Salakhutdinov, R. (2016). Importance weighted autoencoders. In *4th International Conference on Learning Representations (ICLR)*.
- Cremer, C., Morris, Q., and Duvenaud, D. (2017). Reinterpreting importance-weighted autoencoders. *arXiv preprint arXiv:1704.02916*.
- Daudel, K., Benton, J., Shi, Y., and Doucet, A. (2023). Alpha-divergence variational inference meets importance weighted auto-encoders: Methodology and asymptotics. *Journal of Machine Learning Research*, 24(243):1–83.
- Daudel, K. and Roueff, F. (2024). Learning with importance weighted variational inference: Asymptotics for gradient estimators of the vr-iwae bound. *arXiv preprint arXiv:2410.12035*.
- Diao, M., Balasubramanian, K., Chewi, S., and Salim, A. (2023). Forward-backward gaussian variational inference via jko in the bures–wasserstein space. In *Proceedings of the 40th International Conference on Machine Learning*.

- Domke, J. and Sheldon, D. R. (2018). Importance weighting and variational inference. In *Advances in Neural Information Processing Systems*, volume 31.
- Haario, H., Saksman, E., and Tamminen, J. (2001). An adaptive metropolis algorithm. *Bernoulli*, 7(2):223–242.
- Jordan, M., Ghahramani, Z., Jaakkola, T., and Saul, L. K. (1999). An introduction to variational methods for graphical models. *Machine Learning*, 37:183–233.
- Jordan, R., Kinderlehrer, D., and Otto, F. (1998). The variational formulation of the Fokker–Planck equation. *SIAM Journal on Mathematical Analysis*, 29(1):1–17.
- Lambert, M., Chewi, S., Bach, F., Bonnabel, S., and Rigollet, P. (2024). Variational inference via wasserstein gradient flows. In *Proceedings of the 36th International Conference on Neural Information Processing Systems*.
- Li, Y. and Turner, R. E. (2016). Rényi divergence variational inference. In *Advances in Neural Information Processing Systems*, volume 29. Curran Associates, Inc.
- Mnih, A. and Rezende, D. (2016). Variational inference for monte carlo objectives. In *International Conference on Machine Learning*, pages 2188–2196. PMLR.
- Murray, I., Adams, R., and MacKay, D. (2010). Elliptical slice sampling. In Teh, Y. W. and Titterington, M., editors, *Proceedings of the Thirteenth International Conference on Artificial Intelligence and Statistics*, volume 9 of *Proceedings of Machine Learning Research*, pages 541–548, Chia Laguna Resort, Sardinia, Italy. PMLR.
- Rainforth, T., Kosiorek, A., Le, T. A., Maddison, C., Igl, M., Wood, F., and Teh, Y. W. (2018). Tighter variational bounds are not necessarily better. In *International Conference on Machine Learning*, pages 4277–4285. PMLR.
- Ranganath, R., Gerrish, S., and Blei, D. (2014). Black box variational inference. In *Artificial intelligence and statistics*, pages 814–822. PMLR.
- Santambrogio, F. (2015). *Optimal Transport for Applied Mathematicians*. Birkhauser.
- Tan, L. S., Bhaskaran, A., and Nott, D. J. (2020). Conditionally structured variational gaussian approximation with importance weights. *Statistics and Computing*, 30(5):1255–1272.
- Tucker, G., Lawson, D., Gu, S. S., and Maddison, C. J. (2019). Doubly reparameterized gradient estimators for monte carlo objectives. In *Proceedings of the 7th International Conference on Learning Representations*.
- Villani, C. (2009). *Optimal transport: Old and New*. Springer.

# Appendix

This appendix contains additional details and deferred proofs of the theoretical results presented in the main text. Section A contains the proof of the theoretical results. Section B contains the detail derivation of the BW gradient of the VR-IWAE bound.

## A Proofs

### A.1 Proof of Proposition 1

*Proof of Proposition 1.* By exchanging the order of the expectation,  $\mathcal{F}_n(q_n)$  can be expressed as

$$\mathcal{F}_n(q_n) = \mathbb{E}_{\{z_1, \dots, z_K\} \setminus z_n} \underbrace{\mathbb{E}_{z_n \sim q_n} \left[ \log \left( \frac{1}{K} \frac{p(x, z_n)}{q_n(z_n)} + \frac{1}{K} \sum_{i \neq n} w(z_i) \right) \right]}_{=: \mathcal{F}_n^*(q_n)},$$

where the dependency of  $\mathcal{F}_n^*$  on the set of the variables  $\{z_1, \dots, z_K\} \setminus z_n$  is made implicit. Provided that the derivative and the expectation are interchangeable, the Wasserstein gradient of  $\mathcal{F}_n$  can be derived as the Wasserstein gradient of  $\mathcal{F}_n^*$  averaged over the set of the variables  $\{z_1, \dots, z_K\} \setminus z_n$ . To this end, we derive the Wasserstein gradient of  $\mathcal{F}_n^*$ . Recall the derivation of the Wasserstein gradient recapped in Section 2.3. The first variation of  $\mathcal{F}_n^*$  at  $q_n = q$  can be written as

$$\frac{d}{d\epsilon} \mathcal{F}_n^*(q + \epsilon\nu) \Big|_{\epsilon=0} = \frac{d}{d\epsilon} \int_{\mathcal{Z}} \underbrace{\log \left( \frac{1}{K} \frac{p(x, z_n)}{q(z_n) + \epsilon\nu(z_n)} + \frac{1}{K} \sum_{i \neq n} w(z_i) \right)}_{=(*_1)} \underbrace{(q(z_n) + \epsilon\nu(z_n)) dz_n \Big|_{\epsilon=0}}_{=(*_2)},$$

where the right derivative in (3) equals the standard derivative at  $\epsilon = 0$  under sufficient regularity. By exchanging the order of the integral and derivative, it further follows that

$$\frac{d}{d\epsilon} \mathcal{F}_n^*(q_n + \epsilon\nu) \Big|_{\epsilon=0} = \int_{\mathcal{Z}} \left( \left( \frac{d}{d\epsilon} (*_1) \right) \times (*_2) + (*_1) \times \left( \frac{d}{d\epsilon} (*_2) \right) \right) \Big|_{\epsilon=0} dz_n.$$

By standard calculation of derivatives, we have

$$\begin{aligned} (*_1) \Big|_{\epsilon=0} &= \log \left( \frac{1}{K} \sum_{i=1}^K w(z_i) \right), \\ (*_2) \Big|_{\epsilon=0} &= q(z_n), \\ \frac{d}{d\epsilon} (*_1) \Big|_{\epsilon=0} &= -\frac{w(z_n)}{\sum_{i=1}^K w(z_i)} \frac{\nu(z_n)}{q(z_n)}, \\ \frac{d}{d\epsilon} (*_2) \Big|_{\epsilon=0} &= \nu(z_n). \end{aligned}$$

Therefore, the first variation of the functional  $\mathcal{F}_n^*(q_n)$  at  $q_n = q$  results in the following form

$$\delta\mathcal{F}_n^*(z_n) = \log \left( \frac{1}{K} \sum_{i=1}^K w(z_i) \right) - \frac{w(z_n)}{\sum_{i=1}^K w(z_i)} =: f(z_n),$$

where the dependency of the function  $g$  on the set of the variables  $\{z_1, \dots, z_K\} \setminus z_n$  remains made implicit. As the Wasserstein gradient of  $\mathcal{F}_n^*$  is the gradient of the function  $f$ , we have that

$$\begin{aligned} \nabla_{z_n} f(z_n) &= \frac{\nabla_{z_n} w(z_n)}{\sum_{i=1}^K w(z_i)} - \frac{\nabla_{z_n} w(z_n)(\sum_{i=1}^K w(z_i)) - w(z_n)(\nabla_{z_n} \sum_{i=1}^K w(z_i))}{(\sum_{i=1}^K w(z_i))^2} \\ &= \frac{\nabla_{z_n} w(z_n)}{\sum_{i=1}^K w(z_i)} - \frac{\nabla_{z_n} w(z_n)}{\sum_{i=1}^K w(z_i)} + \frac{w(z_n)}{\sum_{i=1}^K w(z_i)} \frac{\nabla_{z_n} w(z_n)}{\sum_{i=1}^K w(z_i)} \\ &= \left( \frac{w(z_n)}{\sum_{i=1}^K w(z_i)} \right)^2 \nabla_{z_n} \log w(z_n). \end{aligned}$$

Hence, taking the expectation of this Wasserstein gradient  $\nabla_{z_n} f(z_n)$  over the implicit dependent variables  $\{z_1, \dots, z_K\} \setminus z_n$  yields the intended form of the Wasserstein gradient of  $\mathcal{F}_n(q_n)$ .  $\square$

## A.2 Proof of Theorem 1

*Proof of Theorem 1.* First, as the  $M$  sets  $\{z_{m,2:K}\}_{m=1}^M$  are i.i.d copies of  $z_{2:K}$ , it is clear that  $\text{SNR}(g_{M,K}^{z_r}(z)) = \sqrt{M} \times \text{SNR}(g_{1,K}^{z_r}(z))$ . Also, we will evaluate  $\text{SNR}(g_{1,K+1}^{z_r}(z))$  rather than  $\text{SNR}(g_{1,K}^{z_r}(z))$ , as both have the same magnitude as  $K \rightarrow \infty$ . Write the former derivative as

$$\begin{aligned} g_{1,K+1}^{z_r}(z) &= \left( \frac{w(z)}{w(z) + \sum_{i=1}^K w_i(z_i)} \right)^2 \frac{\partial}{\partial z_r} \log w(z) \\ &= \left( \frac{w(z)/K}{w(z)/K + p(x) + \frac{1}{K} \sum_{i=1}^K (w_i(z_i) - p(x))} \right)^2 \frac{\partial}{\partial z_r} \log w(z) \\ &= \left( \frac{w(z)/K}{c_K + \frac{1}{K} \sum_{i=1}^K \xi_i} \right)^2 \frac{\partial}{\partial z_r} \log w(z), \end{aligned}$$

where  $c_K := w(z)/K + p(x)$  and  $\xi_i := w_i(z_i) - p(x)$ . We note that  $\xi_i$  are i.i.d. with  $\mathbb{E}(\xi_i) = \int p(x, z) dz - p(x) = 0$ . Denote  $X_K = 1/(c_K + \frac{1}{K} \sum_{i=1}^K \xi_i)^2 = 1/(c_K + \bar{\xi}_K)^2$  with  $\bar{\xi}_K = \frac{1}{K} \sum_{i=1}^K \xi_i$ , we have

$$\text{SNR}(g_{1,K+1}^{z_r}(z)) = \text{SNR}(X_K).$$

Simple calculation gives

$$\mathbb{E}(\bar{\xi}_K^2) = \frac{1}{K} \mathbb{E}(\xi_1^2), \quad \mathbb{E}(\bar{\xi}_K^4) = \frac{1}{K^3} \mathbb{E}(\xi_1^4) + \frac{6(K-1)}{K^3} (\mathbb{E}(\xi_1^2))^2. \quad (13)$$

Applying the Mean Value Theorem to function  $f(x) = 1/(c_K + x)^2$ ,

$$f(x) = f(0) + f'(\zeta)x = c_K^{-2} - 2(c_K + \zeta)^{-3}x,$$

where  $\zeta$  is a value between 0 and  $x$ , we have

$$X_K = c_K^{-2} - \eta_K \bar{\xi}_K$$

with  $\eta_K = 2(c_K + \zeta_K)^{-3}$  for some  $\zeta_K$  between 0 and  $\bar{\xi}_K$ . We have  $c_K^{-2} = p(x)^{-2} + O(1/K)$ , and will show that  $\mathbb{E}(\eta_K \bar{\xi}_K) = O(1/\sqrt{K})$ . As  $\zeta_K$  is between 0 and  $\bar{\xi}_K$ ,  $p(x) + \zeta_K$  is between  $p(x)$  and  $\frac{1}{K} \sum_i w_i(z_i)$ ,

$$\begin{aligned} \eta_K^2 &= \frac{4}{\left(w(z)/K + p(x) + \zeta_K\right)^6} \leq \frac{4}{\left(p(x) + \zeta_K\right)^6} \\ &\leq 4 \max \left\{ \frac{1}{p(x)^6}, \frac{1}{\left(\frac{1}{K} \sum_i w_i(z_i)\right)^6} \right\} \\ &\leq 4 \max \left\{ \frac{1}{p(x)^6}, \frac{1}{K} \sum_i \frac{1}{w_i(z_i)^6} \right\}, \end{aligned}$$

the last inequality is because  $x \mapsto x^{-6}$  is convex in  $(0, \infty)$ . This gives

$$\mathbb{E}(\eta_K^2) \leq 4 \max \left\{ \frac{1}{p(x)^6}, \mathbb{E}(w(Z)^{-6}) \right\} := C < \infty$$

because of Assumption (ii). By the Cauchy-Schwarz theorem, and then using Assumption (i) to bound  $\mathbb{E}(\xi_1^2)$ ,

$$|\mathbb{E}(\eta_K \bar{\xi}_K)| \leq \left( \mathbb{E}(\eta_K^2) \mathbb{E}(\bar{\xi}_K^2) \right)^{1/2} \leq \left( \frac{C}{K} \mathbb{E}(\xi_1^2) \right)^{1/2} = O\left(\frac{1}{\sqrt{K}}\right).$$

Now,

$$|\mathbb{E}(X_K)| = |c_K^{-2} - \mathbb{E}(\eta_K \bar{\xi}_K)| \geq |c_K^{-2} - |\mathbb{E}(\eta_K \bar{\xi}_K)||.$$

As  $c_K^{-2} > 0$  and  $|\mathbb{E}(\eta_K \bar{\xi}_K)| \rightarrow 0$ ,  $c_K^{-2} - |\mathbb{E}(\eta_K \bar{\xi}_K)| > 0$  as  $K$  is large enough, then

$$|\mathbb{E}(X_K)| \geq c_K^{-2} - |\mathbb{E}(\eta_K \bar{\xi}_K)| = 1/p(x)^2 + o(1),$$

which implies

$$|\mathbb{E}(X_K)| = \Omega(1). \tag{14}$$

For the variance term

$$\mathbb{V}(X_K) = \mathbb{E}(X_K^2) - \mathbb{E}(X_K)^2 = \mathbb{E}(\eta_K^2 \bar{\xi}_K^2) - (\mathbb{E}(\eta_K \bar{\xi}_K))^2 \leq \mathbb{E}(\eta_K^2 \bar{\xi}_K^2).$$

Similar to the above, we can show that

$$\mathbb{E}(\eta_K^4) \leq 16 \max \left\{ \frac{1}{p(x)^{12}}, \mathbb{E}(w(Z)^{-12}) \right\} < \infty.$$

Hence, by (13),

$$\mathbb{V}(X_K) \leq \mathbb{E}(\eta_K^2 \bar{\xi}_K^2) \leq \left( \mathbb{E}(\eta_K^4) \mathbb{E}(\bar{\xi}_K^4) \right)^{1/2} = O\left(\frac{1}{K}\right),$$

which implies

$$\frac{1}{\mathbb{V}(X_K)} = \Omega(K). \tag{15}$$

Combining (14)-(15) together, we obtain

$$\text{SNR}(X_K) = \frac{|\mathbb{E}(X_K)|}{\sqrt{\mathbb{V}(X_K)}} = \Omega(\sqrt{K}).$$

This completes the proof.  $\square$

### A.3 Proof of Proposition 3

*Proof of Proposition 3.* By exchanging the order of the expectation,  $\mathcal{G}_n(q_n)$  can be expressed as

$$\mathcal{G}_n(q_n) = \frac{1}{1-\alpha} \mathbb{E}_{z_n \sim q_n} \underbrace{\mathbb{E}_{\{z_1, \dots, z_K\} \setminus z_n} \underbrace{\left[ \log \left( \frac{1}{K} \frac{p(x, z_n)^{1-\alpha}}{q_n(z_n)^{1-\alpha}} + \frac{1}{K} \sum_{i \neq n} w(z_i)^{1-\alpha} \right) \right]}_{=: \mathcal{G}_n^*(q_n)}}$$

where the dependency of  $\mathcal{G}_n^*$  on the set of the variables  $\{z_1, \dots, z_K\} \setminus z_n$  is made implicit. Provided that the derivative and the expectation are interchangeable, the Wasserstein gradient of  $\mathcal{G}_n$  can be derived as the Wasserstein gradient of  $\mathcal{G}_n^*$  averaged over the set of the variables  $\{z_1, \dots, z_K\} \setminus z_n$ . To this end, we derive the Wasserstein gradient of  $\mathcal{G}_n^*$ . Recall the derivation of the Wasserstein gradient recapped in Section 2.3. The first variation of  $\mathcal{G}_n^*$  at  $q_n = q$  can be written as

$$\mathcal{G}_n^*(q + \epsilon \nu) = \underbrace{\frac{d}{d\epsilon} \int_{\mathcal{Z}} \log \left( \frac{1}{K} \frac{p(x, z_n)^{1-\alpha}}{(q(z_n) + \epsilon \nu(z_n))^{1-\alpha}} + \frac{1}{K} \sum_{i \neq n} w(z_i)^{1-\alpha} \right) (q(z_n) + \epsilon \nu(z_n)) dz_n}_{=(*_1)} \Big|_{\epsilon=0} \underbrace{\Big|_{\epsilon=0}}_{=(*_2)}.$$

where the right derivative in (3) equals the standard derivative at  $\epsilon = 0$  under sufficient regularity. By exchanging the order of the integral and derivative, it further follows that

$$\frac{d}{d\epsilon} \mathcal{G}_n^*(q + \epsilon \nu) \Big|_{\epsilon=0} = \int_{\mathcal{Z}} \left( \left( \frac{d}{d\epsilon} (*_1) \right) \times (*_2) + (*_1) \times \left( \frac{d}{d\epsilon} (*_2) \right) \right) \Big|_{\epsilon=0} \times dz_n.$$

By standard calculation of derivatives, we have

$$\begin{aligned} (*_1) \Big|_{\epsilon=0} &= \log \left( \frac{1}{K} \sum_{i=1}^K w(z_i)^{1-\alpha} \right), \\ (*_2) \Big|_{\epsilon=0} &= q(z_n), \\ \frac{d}{d\epsilon} (*_1) \Big|_{\epsilon=0} &= -(1-\alpha) \frac{w(z_n)^{1-\alpha}}{\sum_{i=1}^K w(z_i)^{1-\alpha}} \frac{\nu(z_n)}{q(z_n)}, \\ \frac{d}{d\epsilon} (*_2) \Big|_{\epsilon=0} &= \nu(z_n). \end{aligned}$$

Therefore, the first variation of the functional  $\mathcal{G}_n^*$  at  $q_n = q$  results in the following form

$$\delta \mathcal{G}_n^*(z_n) = \log \left( \frac{1}{K} \sum_{i=1}^K w_i(z_i)^{1-\alpha} \right) - (1-\alpha) \frac{w_n(z_n)^{1-\alpha}}{\sum_{i=1}^K w_i(z_i)^{1-\alpha}} =: g(z_n)$$

where the dependency of the function  $g$  on the set of the variables  $\{z_1, \dots, z_K\} \setminus z_n$  remains made implicit. As the Wasserstein gradient of  $\mathcal{G}_n^*$  is the gradient of the function  $g$ , we have that

$$\nabla_{z_n} g(z_n) = (1 - \alpha) \left( \alpha \frac{w(z_n)^{1-\alpha}}{\sum_{i=1}^K w(z_i)^{1-\alpha}} + (1 - \alpha) \left( \frac{w(z_n)^{1-\alpha}}{\sum_{i=1}^K w(z_i)^{1-\alpha}} \right)^2 \right) \nabla_{z_n} \log w(z_n).$$

Hence, taking the expectation of this Wasserstein gradient  $\nabla_{z_n} g(z_n)$  over the implicit dependent variables  $\{z_1, \dots, z_K\} \setminus z_n$  yields the intended form of the Wasserstein gradient of  $\mathcal{G}_n(q_n)$ .  $\square$

## B Derivations of BW gradient for VR-IWAE bound

This section presents the explicit expression of the BW gradient of the VR-IWAE bound, together with the detailed derivation. Recall that it suffices to consider the Wasserstein gradient of the VR-IWAE bound at the index  $n = K$  as it remains invariant to the choice of the index  $n$ . For notational convenience, let  $G$  denotes the Wasserstein gradient of the VR-IWAE bound at the common variational distribution  $q$ , and let  $g(z_1, \dots, z_K) := w(z_K)^{1-\alpha} / \sum_{i=1}^K w(z_i)^{1-\alpha}$ .

We derive the two terms  $a_*$  and  $S_*$  characterizing the BW gradient of the negative VR-IWAE bound in (12). It follows from (11) and the derivation of the BW gradient recapped in Section 2.4 that

$$\begin{aligned} a_* &= - \mathbb{E}_{z_K \sim q} [G(z_K)] \\ &= - \mathbb{E}_{z_1, \dots, z_K \stackrel{i.i.d.}{\sim} q} [(\alpha g(z_1, \dots, z_K) + (1 - \alpha)g(z_1, \dots, z_K)^2) \nabla_{z_K} \log w(z_K)]. \end{aligned}$$

To establish  $S_*$ , we derive the gradient of  $g(z_1, \dots, z_K)$  with respect to  $z_K$ :

$$\begin{aligned} \nabla_{z_K} g(z_1, \dots, z_K) &= \frac{\nabla_{z_K} w(z_K)^{1-\alpha}}{\sum_{i=1}^K w(z_i)^{1-\alpha}} - \frac{w(z_K)^{1-\alpha} \nabla_{z_K} w(z_K)^{1-\alpha}}{(\sum_{i=1}^K w(z_i)^{1-\alpha})^2} \\ &= (1 - \alpha) \left( \frac{w(z_K)^{1-\alpha}}{\sum_{i=1}^K w(z_i)^{1-\alpha}} - \left( \frac{w(z_K)^{1-\alpha}}{\sum_{i=1}^K w(z_i)^{1-\alpha}} \right)^2 \right) \nabla_{z_K} \log w(z_K) \\ &= (1 - \alpha)(g(z_1, \dots, z_K) - g(z_1, \dots, z_K)^2) \nabla_{z_K} \log w(z_K). \end{aligned}$$

This leads to the explicit expression of the remaining term  $S_*$ :

$$\begin{aligned} S_* &= - \mathbb{E}_{z_K \sim q_K} [\nabla_{z_K} G(z_K)] \\ &= - \mathbb{E}_{z_1, \dots, z_K \stackrel{i.i.d.}{\sim} q} \left[ \nabla_{z_K} \left( \underbrace{(\alpha g(z_1, \dots, z_K) + (1 - \alpha)g(z_1, \dots, z_K)^2)}_{=: (*_1)} \underbrace{\nabla_{z_K} \log w(z_K)}_{=: (*_2)} \right) \right] \\ &= - \mathbb{E}_{z_1, \dots, z_K \stackrel{i.i.d.}{\sim} q} [(\nabla_K(*_1))(*_2) + (*_1)(\nabla_K(*_2))]. \end{aligned}$$

Here, using the expression of  $\nabla_{z_K} g(z_1, \dots, z_K)$ , we have

$$\begin{aligned} \nabla_K(*_1) &= \alpha \nabla_{z_K} g(z_1, \dots, z_K) + 2(1 - \alpha)g(z_1, \dots, z_K) \nabla_{z_K} g(z_1, \dots, z_K) \\ &= \left( (1 - \alpha)(g(z_1, \dots, z_K) - g(z_1, \dots, z_K)^2) (\alpha + 2(1 - \alpha)g(z_1, \dots, z_K)) \right) \nabla_{z_K} \log w(z_K). \end{aligned}$$

Plugging  $\nabla_K(*_1)$  in together with  $\nabla_K(*_2) = \nabla_{z_K}^2 \log w(z_K)$  completes the derivation.